Technical Note

Acoustic Matching Characteristics of Annular Piezoelectric Ultrasonic Sensor

Haoran LI[(1)], Yan HU[(2)*], Laibo LI[(1)], Dongyu XU[(2), (3)*]

[(1)] *Shandong Provincial Key Lab of Preparation and Measurement of Building Materials, University of Jinan*
Jinan 250022, PR China

[(2)] *School of Civil Engineering, Central South University*
Changsha 410075, PR China

[(3)] *School of Civil Engineering and Architecture, Linyi University*
Linyi 276000, PR China
*Corresponding Authors' e-mails: csyhuy@csu.edu.cn (Yan HU); xudongyu@lyu.edu.cn (Dongyu XU)

Using intelligent materials and sensors to monitor the safety of concrete structures is a hot topic in the field of civil engineering. In order to realize the omni-directional monitoring of concrete structural damage, the authors of this paper designed and fabricated an embedded annular piezoelectric ultrasonic sensor using the annular piezoelectric lead zirconate titanate (PZT) ceramic as a sensing element and epoxy resin as the matching and the backing layers. The influence of different matching and backing layers thickness on the acoustic characteristic parameters of the sensor were studied. The results show that the resonant frequency corresponding to the axial mode of annular piezoelectric ceramics moves toward the high frequency direction with the decrease of the height of piezoelectric ceramics, and the radial vibration mode increases as well as the impedance peak. With the thickness of the backing layer increases from 1 mm to 2 mm, the radial resolution of the annular piezoelectric ultrasonic sensor is enhanced, the pulse width is reduced by 39% comparing with the sensors which backing layer is 1 mm, and the head wave amplitude and −3 dB bandwidth are increased by 61% and 66%, respectively. When the matching layer thickness is 3 mm, the sensor has the highest amplitude response of 269 mV and higher sensitivity.

Keywords: piezoelectric ceramics; ultrasonic sensors; acoustic matching characteristics.

1. Introduction

Concrete is one of the most important building materials in construction engineering, and its quality is directly related to the safety of building structures (BASU *et al.*, 2021; LIU *et al.*, 2020). Using intelligent materials or structures to carry out nondestructive testing and health monitoring on concrete structures is an important means to ensure their safety (CHENG *et al.*, 2013; GENG *et al.*, 2017; LIU *et al.*, 2020; XU *et al.*, 2021). At present, the commonly used concrete evaluating methods include a sampling method, rebound method, post-loading pull out testing method, ultrasonic method and so on. Among them, the ultrasonic method has the advantages of good repeatability and no damage to the concrete

structure, which is favoured by the majority of scholars (RIDENGAOQIER *et al.*, 2021; HAM *et al.*, 2017; LOOTENS *et al.*, 2020; MIRÓ *et al.*, 2021; RAO, SASMAL, 2020).

At present, many scholars have made outstanding contributions in the field of ultrasonic evaluations of concrete. For example, Lee proposed a new model based on the ultrasonic pulse velocity method, to predict the relationship between the setting time and the compressive strength of concrete (LEE, LEE, 2020). HONG *et al.* (2020) used the non-contact ultrasonic system to study the hardening of concrete under accelerated curing conditions. SUN and ZHU (2020) proposed a method for detecting honeycomb and cavity around concrete using cross tie rods as waveguides. NEMATZADEH *et al.* (2021) used the ultrasonic pulse

velocity method to characterize the mechanical properties of steel fiber reinforced concrete (SFRC) containing reclaimed nylon particles and natural zeolite. ZHANG et al. (2017) used the ultrasonic array method to detect the change of the elastic modulus field of concrete damaged by sulfate erosion and loading GUO et al. (2016) proposed the nondestructive ultrasonic scattering technique to measure the gap ruler distribution in hardened concrete samples. The results show that the ultrasonic scattering technique could evaluate the freeze-thaw durability of concrete by measuring the size of the void in concrete. CHOI et al. (2016) used the ultrasonic pulse echo method to detect the horizontal cracking or delamination of concrete pavement slabs.

It is well known that ultrasonic transducers made of piezoelectric materials play an important role in the ultrasonic testing technology. For example, TSENG and WANG (2004) studied the application of intelligent PZT sensors in damage detection and evolution of concrete. SHIN and OH (2009) used electromechanical impedance sensing technology to study the application of intelligent PZT patches in the monitoring of concrete strength development. The core of ultrasonic detection technology of concrete structure is an ultrasonic sensor. At present, the components used in the ultrasonic sensor are mainly piezoelectric ceramics polarized along the thickness direction, which are only sensitive to the damage stress wave in a specific direction, and can not realize the all-directional damage detection of concrete structure. The annular piezoelectric ultrasonic sensor based on the radial polarization of annular piezoelectric ceramics has the advantage of horizontal nondirectivity. Therefore, in this paper, an embedded annular piezoelectric ultrasonic sensor was designed and prepared, and an ultrasonic test platform was built to investigate the influence of the matching and backing layers on the acoustic impedance, pulse duration and the head wave amplitude of the proposed sensor.

2. Theoretical background

The impedance and thickness of the matching layer have great influence on the sensitivity, bandwidth, transfer function and pulse waveform of the sensor.
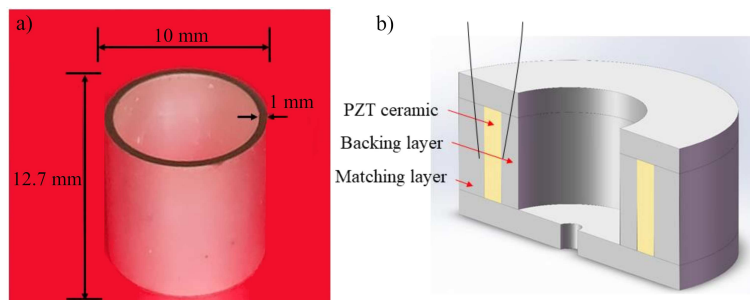
When the piezoelectric ceramic is excited by an electrical signal, vibration will be generated on the interface between the matching layer and the piezoelectric ceramic, and the vibration is coupled to the load through the matching layer. According to the transmission theory (YANG et al., 2020), the input impedance Z_{A1} on the interface is:

$$Z_{A_1} = Z_1 \frac{Z_L \cos k_1 \delta_1 + j Z_1 \sin k_1 \delta_1}{Z_1 \cos k_1 \delta_1 + j Z_L \sin k_1 \delta_1}, \qquad (1)$$

where k_1 is the circular wave number in the matching layer, δ_1 [mm] is the matching layer thickness. Z_1 [Ω] is the matching layer impedance, Z_L [Ω] is the load impedance.

It can be seen from Eq. (1) that the input impedance at the interface is a function of frequency and will change as the frequency changes. The acoustic impedance matching is achieved when the matching layer thickness $\delta_1 = \frac{\lambda_1}{4}$ and the acoustic impedance is $\sqrt{Z_0 Z_L}$, where λ_1 [m] is the wavelength, Z_0 [Ω] is the acoustic impedance of piezoelectric ceramics.

3. Experiment

3.1. The structural design of ultrasonic sensor

Generally, the damage frequency of concrete structures ranges from 20 kHz to 200 kHz (LIU et al., 2017). Therefore, PZT-5 annular piezoelectric ceramics (Zibo Yuhai Electronic Ceramics Co. Ltd., China) with a frequency of 200 kHz were used in this paper with a height of 12.7 mm and a wall thickness of 1 mm. The detailed parameters are shown in Table 1.

Table 1. Properties of annular piezoelectric ceramic.

Ceramic	d_{33} [pC·N^{-1}]	ε_r	k_p [%]	k_t [%]	Q_m
PZT-5	620	3200	0.68	0.52	70

Note: d_{33} – piezoelectric strain factor; ε_r – relative permittivity; k_p – planar electromechanical coupling coefficient; k_t – thickness electromechanical coupling coefficient; Q_m – mechanical quality factor.

Figure 1 is a photograph of annular piezoelectric ceramic and a section view of the annular piezoelectric ultrasonic sensor composed of annular piezoelectric ce-

Fig. 1. Photo of annular piezoelectric ceramics and structural profile of the sensor.

ramics, matching and backing layers. The epoxy resin was used to prepare matching and backing layer of the sensor because it has the characteristics of good fluidity and high strength after curing. The effects of different acoustic matching conditions on the acoustic impedance, pulse duration and head wave amplitude of the annular piezoelectric ultrasonic sensor were studied by changing the thickness of the matching and the backing layers.

The mixture of tungsten powder and epoxy resin was used as the sensor's matching layer material. The ultrasonic velocity of sound in this kind of material is about 2.68 km/s. Some researchers have shown that when the matching layer thickness conforms to the quarter-wavelength theory, the amplitude loss is minimal when the sound wave penetrates. The length of a quarter wavelength refers to a quarter of the wavelength of ultrasonic wave propagation in the matched layer material, as shown in the formula below:

$$\delta_1 = \frac{\lambda}{4} = \frac{v}{4f}, \tag{2}$$

where δ_1 [mm] is the thickness of matching layer, λ [m] is the wavelength, v [m/s] is the speed of ultrasonic waves when travel through the water, f [kHz] is the resonant frequency of piezoelectric ceramics.

The resonant frequency of selected piezoelectric ceramics is in the vicinity of 160 kHz. Putting it into the above formula indicates that the theoretical optimal matching layer is about 3.35 mm. So the matching layers with four different thicknesses, that is 1 mm, 2 mm, 3 mm, and 3.5 mm were designed. The range about matching layer thickness span is moderate so that the influence of the thickness of the matching layer on the performance of the sensor can be seen more obviously.

Here, eight ultrasonic sensors with different acoustic matching conditions were designed, as shown in

Table 2. Because the wall thickness of the annular piezoelectric ceramic is 1 mm, two matching layer thicknesses were designed, which is 1 mm, 2 mm, respectively. Therefore, based on the above principles, four matching layer thicknesses and two backing layer thicknesses were designed, and the total prepared eight ultrasonic sensors with different acoustic matching conditions, as shown in Table 2.

Table 2. Parameters of matching and backing layers of the sensors.

Sensor number	1	2	3	4	5	6	7	8
Thickness of backing layer [mm]	1	1	1	1	2	2	2	2
Thickness of matching layer [mm]	1	2	3	3.5	1	2	3	3.5

In order to ensure the accuracy of the matching and the backing layers, the mold by using polytetrafluoroethylene (PTFE) was designed, as shown in Fig. 2. Figure 2a is the structure view of the mold, and Fig. 2b is the section view of the mold. Among them, part 1 is a mold sleeve, and the diameter of its center hole has four specifications: 12 mm, 14 mm, 16 mm, and 17 mm, which are used to change the thickness of the matching layer of the sensor. As shown in Fig. 2b, there is a groove with width of 2.5 mm and depth of 20 mm on the outside of part 1, which is used to connect with the mold base. Part 2 is a cylindrical structure with a diameter of 7 mm and 5 mm, which is used to change the thickness of the backing layer of the sensor. Part 2 is slotted at the bottom for easy fixing on the mold base. Part 3 is the base of the mold. As it is shown in Fig. 2a, there is a groove with the depth of 0.5 mm and width of 1 mm in the center, which is convenient for fixing the annular piezoelectric ceramics so that the piezoelectric ceramics are located in the center.
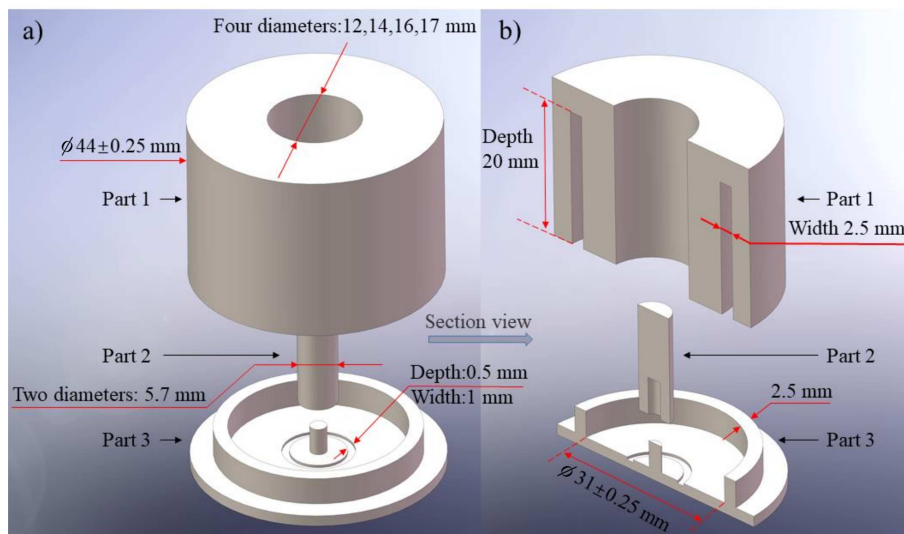

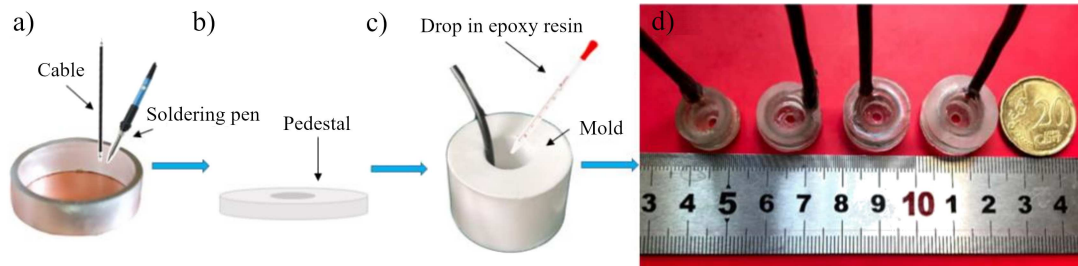Fig. 2. The mold's structure and section view.

Fig. 3. The sensor preparation process.

3.2. Sensor preparation

The annular piezoelectric ceramic has radial and axial vibration modes, which can be observed through electrical impedance spectra. In order to study the influence of the height of annular piezoelectric ceramic on its electrical impedance, annular piezoelectric ultrasonic sensors of 12.70 mm, 5.24 mm, 3.68 mm, and 1.86 mm in height were prepared. The detailed preparation process is shown in Fig. 3.

First, as shown in Fig. 3a, the wire was welded on the positive and negative electrodes of the annular piezoelectric ceramics. Then, the epoxy resin was used to make a pedestal with the thickness of 2 mm, as shown in Fig. 3b, which can block water. In Fig. 3c, the ceramics was put in the center of the base, and connected the mold sleeve with the base. The epoxy resin was filled into the mold to prepare matching and backing layers of annular piezoelectric ceramics. Figure 3d shows the photos of the sensors.

3.3. Performance test

The impedance analyzer (E400A, Keysight, USA) was used to test the electrical impedance of the PZT ceramics. The ultrasonic test platform, as shown in Fig. 4a, was set up to study the directivity and acoustic propagation characteristics of the annular piezoelectric ultrasonic sensor in water. The signal generator (AFG3022B, Tektrontek, USA) was used to excite annular piezoelectric ultrasonic sensor to produce ultrasonic signals. The ultrasonic sensor (100K-P40F, Shan-

tou Ultrasonic Co. Ltd., China) was used to capture ultrasonic signal, and the oscilloscope (MDO3024, Tektrontek, USA) was used to record the ultrasonic wave transmitted in water. In this part, the annular sensor was put in the center of the water tank, and the 100K-P40F sensor was put around the annular sensor. In the direction of 30, 60, 90, 120 degrees, all the way up to 330, 360 degrees. The emission performance of the annular sensor in all directions was tested. At each angle, the first amplitude was tested four times and average it.

The ultrasonic test platform, as shown in Fig. 4b, was built to study the acoustic propagation characteristics of the annular piezoelectric ultrasonic sensor in the epoxy resin and steel rods. The annular piezoelectric ultrasonic sensor emitted ultrasonic signal, and the commercial sensor received the ultrasonic signal. In order to avoid the influence of contacting force between the sensors and solid medium on the amplitude of the ultrasonic signal, a fixture was designed to fix the sensors and the solid medium. Additionally, the pulse width, the head wave amplitude and the peak-to-peak value of annular piezoelectric ultrasonic sensor under different acoustic matching conditions were also studied. The pulse width is the period in which the pulse can reach its maximum value. The head wave amplitude means the magnitude of the first pulse. The peak-to-peak value refers to the difference between the highest and lowest signal values in a cycle, which is the range between the maximum and minimum. It describes the size of the range of signal values.
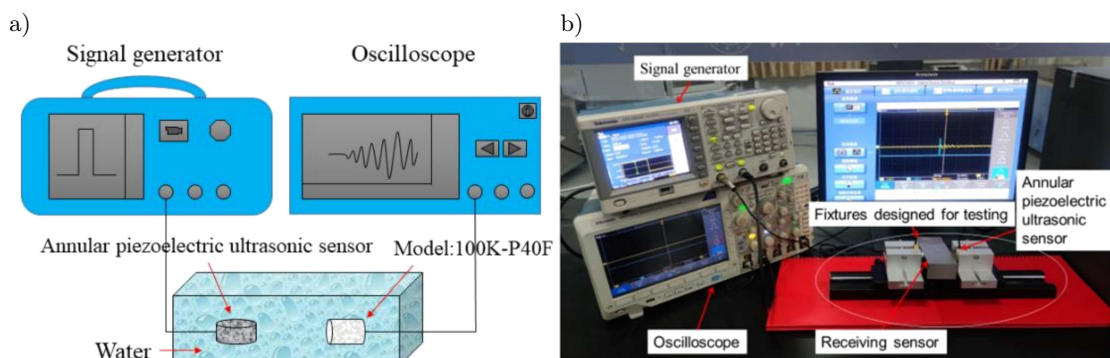

Fig. 4. The ultrasonic test platform.

4. Results and discussion

4.1. Impedance spectra analysis

Figure 5 shows the impedance spectrum of annular piezoelectric ceramics. As can be seen from the figure, each annular piezoelectric ceramic has two obvious impedance peaks, among which the resonance peak near 200 kHz is the radial mode resonance peak. Since the radial size of the annular piezoelectric ceramic remains unchanged, the corresponding radial resonance frequency does not change with the height, but the radial resonance peak value increases gradually with the decrease of the height. The reason may be that the lower the height of piezoelectric ceramics, the weaker the ability to suppress the radial mode, so the radial vibration is enhanced. The radial resonance peak value of the annular piezoelectric ceramics with a height of 1.8 mm is the largest of 18 kΩ, and that of the annular piezoelectric ceramics with a height of 12.7 mm is the smallest of 4.2 kΩ.
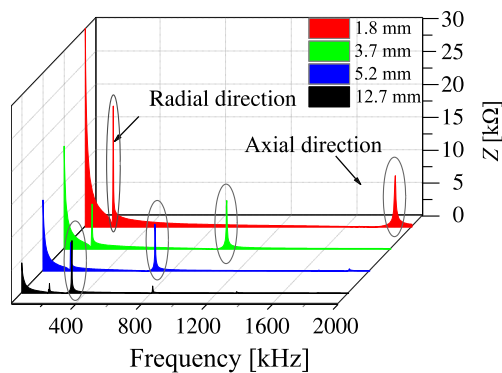

Fig. 5. Impedance spectrum of annular piezoelectric ceramics.

In addition, it also can be seen from the figure that the axial resonant peak gradually moves to the high frequency direction as the height of the piezoelectric ceramics decreases. The axial resonant frequency of the circular piezoelectric ceramics with heights of 1.8 mm, 3.7 mm, 5.2 mm, and 12.7 mm appear around 1.9 MHz, 1.2 MHz, 700 kHz, and 300 kHz, respectively, but the axial resonant peak value is basically the same, which is about 7 kΩ. According to the definition of frequency constant of piezoelectric materials, the product of thickness and the axial resonant frequency of the same kind piezoelectric material should be a constant value. Therefore, when the height of the annular piezoelectric ceramics decreases, its axial resonant frequency increases.

By contrast, the height of the annular piezoelectric ceramic may influence its axial mode corresponding to the resonance frequency and the radial mode corresponding to the impedance of the peak. Based on the frequency range of different vibration modes, the radial vibration of annular piezoelectric ceramic was mainly

considered in this paper, and the annular piezoelectric ceramics with a height of 3.7 mm was used to prepare the ultrasonic sensor.

4.2. Acoustic propagation characteristics of sensor in water

Figure 6a shows the change of the head wave amplitude of #1–#4 ultrasonic sensors as a function of receiving angle. It can be seen from the figure that the head wave amplitude received by the same sensor does not change significantly with the receiving angle. Since we do not have a fixture to fix the sensor in water, the amplitude of the head wave received by the sensor will vary slightly at different angles for the same sensor. But as for the different sensors, the different backing and matching layers lead to the different amplitude of head wave. The average head wave amplitude of the #1–#4 sensors is 300 mV, 350 mV, 330 mV, and 340 mV, respectively, and the #2 sensor with a matching layer thickness of 2 mm has the largest head wave amplitude. The average of first wave amplitude about these four types of sensors is 330 mV.
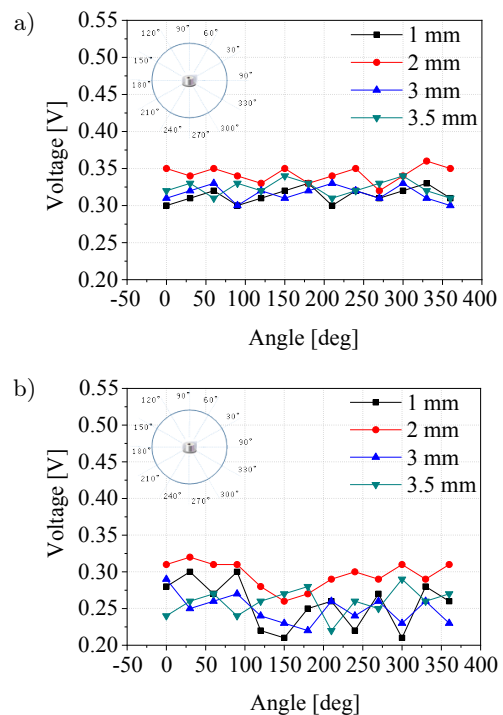

Fig. 6. Head wave amplitude as a function of receiving angle of the sensors.

Figure 6b shows the variation of the head wave amplitude of #5–#8 ultrasonic sensors when the receiving angle changed. The average of first wave amplitude about #5–#8 sensors is 283 mV. Compared with sensors of #1–#4, the average head wave amplitude of sensors #5–#8 decreases by 14%. The reason is that the thicker the backing layer is, the inhibition effect on the vibration of the annular piezoelectric ceramics

will be more obvious, so the amplitude of the head wave decreases with the increase of the backing layer thickness. According to Figs 6a and 6b, the annular piezoelectric ultrasonic sensor can transmit ultrasonic signals uniformly and stably in radial direction, accordingly realize the horizontal nondirectivity.

Figure 7a shows the waveform changes of #1–#4 ultrasonic sensors when the thickness of the backing layer is 1 mm. The number of wave peak about #1–#4 sensors is 7 times, 4 times, 12 times and 6 times, respectively, and the average number of wave peak is four. Figure 7b shows the waveform changes of #5–#8 ultrasonic sensors when the thickness of the backing layer is 2 mm. The number of wave peak about #5–#8 sensor is 2 times, 4 times, 3 times, and 4 times, respectively, and the average number of wave peak decreases to two. The reason is that with the increase of the thickness of the backing layer, the damping effect of the backing layer on the ultrasonic sensor in-creases gradually, and the vibration suppression effect to the piezoelectric ceramic is more obvious. The annular piezoelectric ceramic is excited by the electric signal to produce vibration. If there is no backing layer, when the electric signal stops the excitation, the annular piezoelectric ceramic will not stop the vibration immediately, but it will take a period of time to stop the vibration, the pulse wave is much longer than the excitation pulse, and the pulse echo lasts longer, which will reduce the resolution of the annular piezoelectric ultrasonic sensor. Therefore, it can be seen that the backing layer of the annular piezoelectric ultrasonic sensor improves the radial resolution of the transducer.

Figure 8a is the peak-to-peak value and the head wave amplitude of #1–#8 ultrasonic sensors. It can be seen that the peak-to-peak values of sensors showed a trend of first increasing and then decreasing, and the #7 sensor with a matching layer thickness of 3 mm has the largest peak-to-peak value of 269 mV. Also, it has the largest amplitude of head wave of 68 mV. The reason is that when the thickness of the matching layer is 3 mm, ultrasonic has the best penetration. The best acoustic matching condition is achieved among piezo-electric ceramics, matching layer and water medium. The amplitude of the head wave of the ultrasonic wave reflected the sensitivity of the ultrasonic sensor and in-dicates the amount of energy lost when the ultrasonic
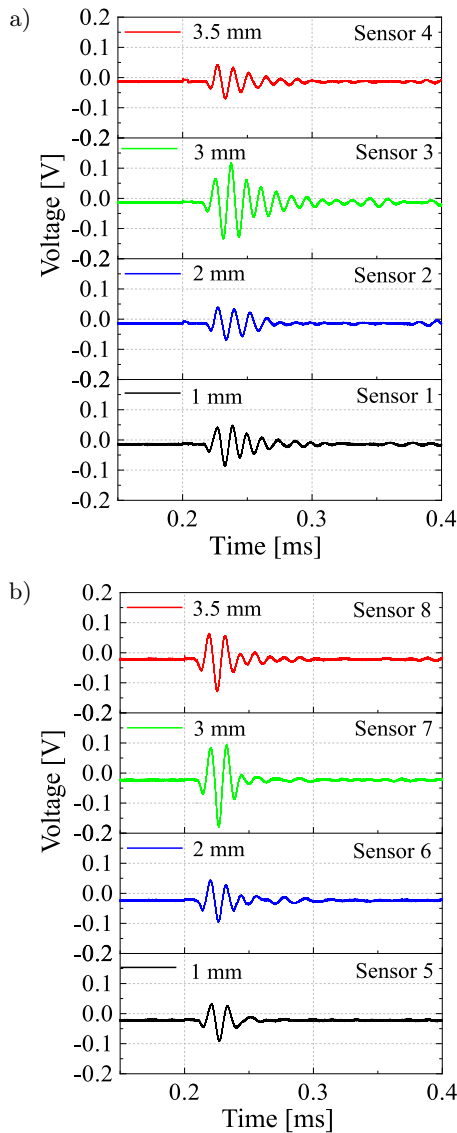

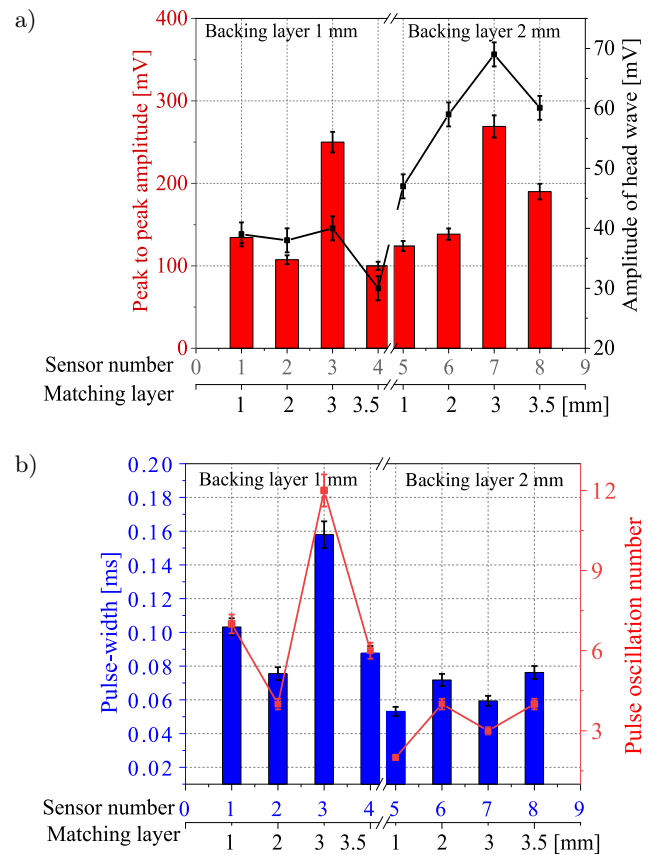Fig. 7. Time-domain diagram of ultrasonic waves in water.

Fig. 8. The peak-to-peak values and head wave amplitudes of #1–#8 sensors in water.

wave penetrates the matching layer. It can also be seen from Fig. 8a that when the thickness of backing layer is 1 mm, the average head wave amplitude is 36 mV, and which is 58 mV when the backing layer thickness is 2 mm, the amplitude increased by 61% than that of the sensor with the backing layer thickness of 1 mm.

Figure 8b shows the variation of waveform duration time and oscillation times of #1–#8 ultrasonic sensors. The #3 sensor has the maximum waveform duration time, approaching 0.16 ms. This is because its backing layer has a lower mass, so it has less inhibition on the sensor. At the same time, the thickness of 3 mm matching layer is the best matching condition. Therefore, #3 sensor has a larger peak-to-peak value and a longer waveform duration time. The average waveform duration time is 0.106 ms for #1–#4 sensors, and 0.065 ms for #5–#8 sensors, reduced by 39% than that of #1–#4 sensors. The reason is that the mass of the backing layer of #5–#8 sensors is larger, accordingly has more obvious inhibition effect. Additionally, we can see from Fig. 8b that #7 sensor has fewer oscillation times than other sensors. The reason is that #7 sensor has 2 mm backing layer and 3 mm matching layer, which means it has the largest mass load that can prevent sensor vibration for a long time. It can also be seen from Fig. 8b that the average oscillation times is 7.25 for #1–#4 sensors, and 3.25 for #5–#8 sensors, approximately 55% less than #1–#4 sensors. It means that the increase of backing layer thickness improves the radial resolution of the transducer.

Figures 9 and 10 are the Fourier transform spectra when the thickness of the backing layer is 1 mm and 2 mm, respectively. It can be seen from the figure that the average dominant frequency of #1– #8 sensors is 80 kHz. #3 sensor dominant frequency is the highest, which is 88 kHz, while the dominant frequency of #5 sensor is the lowest, which is 64 kHz, this may be caused by the too small thickness of the matching layer of the #5 sensor. Excluding the #5 sensor, the average dominant frequency of other sensors is 82 kHz. As for the peak value, #5 sensor is the smallest, which is 11.5 mV, while the peak value of the #7 sensor is the largest, which is 20 mV. At this time, the acoustic matching condition of the #7 sensor is 2 mm of the backing layer and 3 mm of the matching layer. The −3 dB bandwidth indicates the frequency bandwidth when the amplitude is $\sqrt{2}/2$ times of the maximum value. In this work, the average −3 dB bandwidth of #1–#4 sensors is 18 kHz, and the average −3 dB bandwidth of #5–#8 sensors is 30 kHz. Compared with the #1–#4 sensor with a backing layer of 1 mm, the −3 dB bandwidth of #5–#8 sensors is increased by 66%, indicating that the backing layer can significantly increase the −3 dB bandwidth of the sensor. Among them, the −3 dB bandwidth of #7 sensor is the largest, which is 31 kHz. This may be because the matching layer thickness of 3 mm is the most beneficial to the propagation
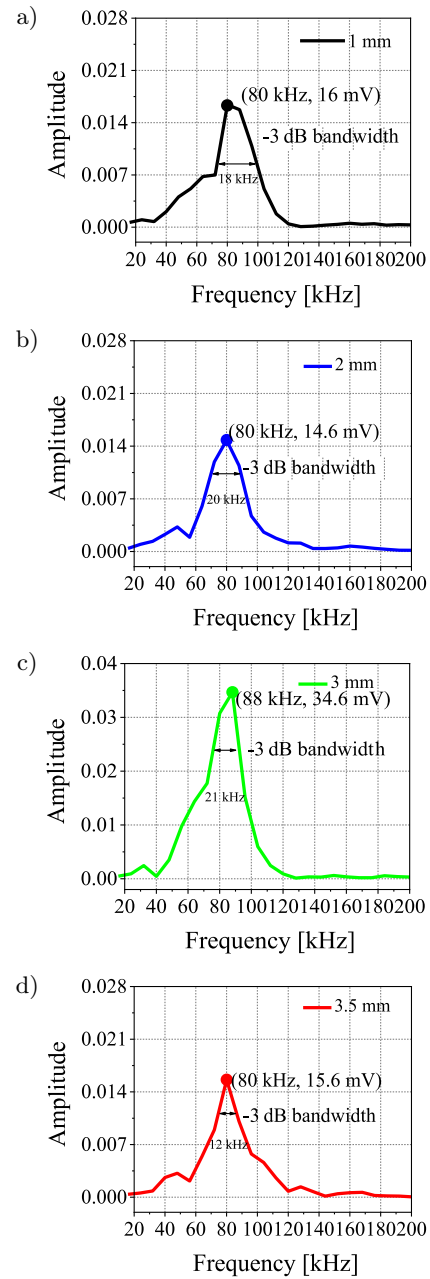

Fig. 9. Spectrogram of the backing layer thickness of 1 mm.

of ultrasonic waves, and the sensor has the highest sensitivity, so it has the largest ultrasonic amplitude and the largest bandwidth.

4.3. Acoustic propagation characteristics of the sensor in the epoxy resin and steel

When the thickness of the backing layer is 2 mm, the annular piezoelectric ultrasonic sensor has a strong radial resolution. Therefore, #5–#8 sensors are selected, and the epoxy resin and steel block are used as the propagation medium to test the acoustic propagation characteristics of the ultrasonic sensor in the solid. In order to reduce the error caused by human
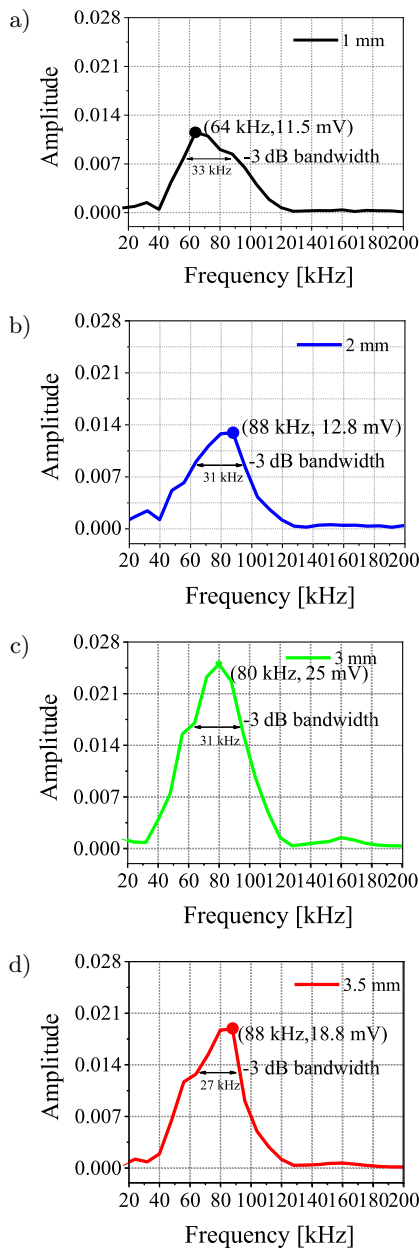
Fig. 10. Spectrogram of the backing layer thickness of 2 mm.

Fig. 11. Time-domain diagram of ultrasonic waves in epoxy resin (a) and steel (b).

factors, the annular piezoelectric ultrasonic sensor was fixed on the fixture, and the sound propagation medium in the middle is the epoxy resin and steel block, respectively.

Figures 11a and 11b show the ultrasonic time-domain spectra of the sensor in the epoxy resin and steel medium, respectively. It can be seen from Fig. 11a that the pulse duration of #5 sensor is the longest and the amplitude is the lowest, and #7 sensor has the largest peak-to-peak value which can reach 87 mV. Meanwhile, the pulse width is very narrow. The above results show that #7 sensor has the best acoustic matching condition. It can be seen from Fig. 11b that the ultrasonic attenuation is slow in the steel medium.
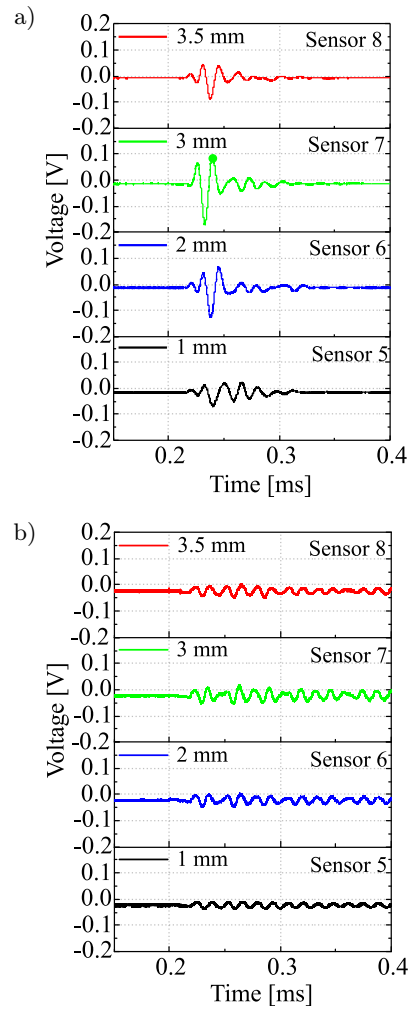
The reason may be that when the epoxy resin is a matching layer, it cannot solve the impedance matching problem between the sensor and the steel medium. On the other hand, the steel is a metal. It is characterized by high impedance, high sound velocity and low attenuation, so the ultrasonic attenuation is slow.

Figure 12 shows the changing tendency of peak-to-peak value and head wave amplitude when #5–#8 sensors work on the epoxy resin and steel medium, respectively. It can be seen from Fig. 12a that when working in the epoxy resin medium, the peak-to-peak value of #7 sensor is the largest, which is 252 mV, and the head wave amplitude is the largest, which is 7.5 mV. It can be seen from Fig. 12 that when the annular ultrasonic sensor prepared in this paper works in a solid medium, the peak-to-peak value and the head wave amplitude both increase first and then decrease. One of the purposes of adding a matching layer is to enable the ultrasonic transducer to achieve high sensitivity, reduce the reflection of ultrasonic waves on the surface of the working medium, and improve the effective transmission energy of ultrasonic waves. The matching layer of
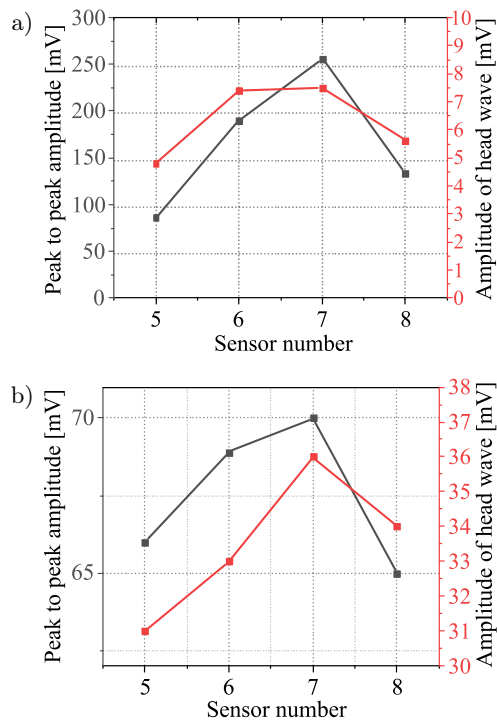
a)

b)

Fig. 12. The peak-to-peak values and head wave amplitudes of #5–#8 sensors when working in the epoxy resin (a) and steel (b).

3 mm thickness designed in this paper can make the sensor obtain the highest amplitude response and sensitivity.

5. Conclusion

In this paper, a kind of annular piezoelectric ultrasonic sensor was designed and fabricated using annular piezoelectric ceramic. The influence of matching and backing layer with different thickness on the acoustic characteristic parameters of the ultrasonic sensor was studied. The following conclusions are drawn:

1) The height of annular piezoelectric ceramics mainly affects the resonance frequency corresponding to the axial mode and the impedance peak corresponding to the radial mode. As the height of the piezoelectric ceramic decreases, the resonance frequency corresponding to the axial mode of the annular piezoelectric ceramic moves to the high frequency direction, and the radial vibration mode as well as the impedance peak value increases.

2) With the thickness of the backing layer increasing, the vibration suppression effect on piezoelectric ceramics is enhanced. When working in water, the head wave amplitude of a sensor with a backing layer of 2 mm is reduced by an average of 14% compared with a sensor with a backing layer of 1 mm.

3) With the increase of the backing layer, the average pulse width of the sensor is decreased by 39%, indicating that the backing layer can improve the radial resolution of the sensor. At the same time, with the increase of the backing layer, the −3 dB bandwidth about the sensor is increased by 66%, indicating that the −3 dB bandwidth can be significantly improved by increasing the backing layer thickness.

4) When the thickness of the matching layer and the backing layer are 3 mm and 2 mm, respectively, the ultrasonic sensor can obtain the highest amplitude response and sensitivity. The amplitude can reach 269 mV when working in water and 252 mV when working in the epoxy resin medium.

Acknowledgments

References

1. BASU S., THIRUMALAISELVI A., SASMAL S., KUNDU T. (2021), Nonlinear ultrasonics-based technique for monitoring damage progression in reinforced concrete structures, *Ultrasonics*, **115**, doi: 10.1016/j.ultras.2021. 106472.

2. CHENG X., QIN L., ZHONG Q.Q., HUANG S.F., LI Z.J. (2013), Temperature and boundary influence on cement hydration monitoring using embedded piezoelectric transducers, *Ultrasonics*, **53**(2): 412–416, doi: 10.1016/j.ultras.2012.07.007.

3. CHOI P., KIM D.-H., LEE B.-H., WON M.C. (2016), Application of ultrasonic shear-wave tomography to identify horizontal crack or delamination in concrete pavement and bridge, *Construction and Building Materials*, **121**: 81–91, doi: 10.1016/j.conbuildmat.2016.05.126.

4. GENG B., XU D., YI S., GAO G., XU H., CHENG X. (2017), Design and properties 1–3 multi-element piezoelectric composite with low crosstalk effects, *Ceramics International*, **43**(17): 15167–15172, doi: 10.1016/ j.ceramint.2017.08.047.

5. GUO S., DAI Q., SUN X., SUN Y. (2016), Ultrasonic scattering measurement of air void size distribution in hardened concrete samples, *Construction and Building Materials*, **113**: 415–422, doi: 10.1016/j.conbuild mat.2016.03.051.

6. HAM S., SONG H., OELZE M.L., POPOVICS J.S. (2017), A contactless ultrasonic surface wave approach to characterize distributed cracking damage in concrete, *Ultrasonics*, **75**: 46–57, doi: 10.1016/j.ultras.2016.11.003.

7. HONG J., KIM R., LEE C.H., CHOI H. (2020), Evaluation of stiffening behavior of concrete based on contactless ultrasonic system and maturity method, *Construction and Building Materials*, **262**, doi: 10.1016/ j.conbuildmat.2020.120717.

8. Lee T., Lee J. (2020), Setting time and compressive strength prediction model of concrete by nondestructive ultrasonic pulse velocity testing at early age, *Construction and Building Materials*, **252**: 119027, doi: 10.1016/j.conbuildmat.2020.119027.

9. Liu P., Hu Y., Chen Y., Geng B., Xu D. (2020), Investigation of novel embedded piezoelectric ultrasonic transducers on crack and corrosion monitoring of steel bar, *Construction and Building Materials*, **235**: 117495, doi: 10.1016/j.conbuildmat.2019.117495.

10. Liu P., Hu Y., Geng B., Xu D. (2020), Corrosion monitoring of the reinforced concrete by using the embedded annular piezoelectric transducer, *Journal of Materials Research and Technology*, **9**(3): 3511–3519, doi: 10.1016/j.jmrt.2020.01.088.

11. Liu P., Wang W., Chen Y., Feng X., Miao L. (2017), Concrete damage diagnosis using electromechanical impedance technique, *Construction and Building Materials*, **136**: 450–455, doi: 10.1016/j.conbuildmat.2016.12.173.

12. Lootens D. *et al.* (2020), Continuous strength measurements of cement pastes and concretes by the ultrasonic wave reflection method, *Construction and Building Materials*, **242**: 117902, doi: 10.1016/j.conbuildmat.2019.117902.

13. Miró M., Eiras J.N., Poveda P., Climent M.Á., Ramis J. (2021), Detecting cracks due to steel corrosion in reinforced cement mortar using intermodulation generation of ultrasonic waves, *Construction and Building Materials*, **286**: 122915, doi: 10.1016/j.conbuildmat.2021.122915.

14. Nematzadeh M., Tayebi M., Samadvand H. (2021), Prediction of ultrasonic pulse velocity in steel fiber-reinforced concrete containing nylon granule and natural zeolite after exposure to elevated temperatures, *Construction and Building Materials*, **273**: 121958, doi: 10.1016/j.conbuildmat.2020.121958.

15. Rao R.K., Sasmal S. (2020), Smart nano-engineered cementitious composite sensors for vibration-based health monitoring of large structures, *Sensors and Actuators A: Physical*, **311**: 112088, doi: 10.1016/j.sna.2020.112088.

16. Ridengaoqier E., Hatanaka S., Palamy P., Kurita S. (2021), Experimental study on the porosity evaluation of pervious concrete by using ultrasonic wave testing on surfaces, *Construction and Building Materials*, **300**: 123959, doi: 10.1016/j.conbuildmat.2021.123959.

17. Shin S.W., Oh T.K. (2009), Application of electromechanical impedance sensing technique for online monitoring of strength development in concrete using smart PZT patches, *Construction and Building Materials*, **23**(2): 1185–1188, doi: 10.1016/j.conbuildmat.2008.02.017.

18. Sun H., Zhu J. (2020), Nondestructive evaluation of steel-concrete composite structure using high-frequency ultrasonic guided wave, *Ultrasonics*, **103**: 106096, doi: 10.1016/j.ultras.2020.106096.

19. Tseng K.K., Wang L. (2004), Smart piezoelectric transducers for in situ health monitoring of concrete, *Smart Material Structures*, **13**(5): 1017–1024, doi: 10.1088/0964-1726/13/5/006.

20. Xu Y., Wang Q., Jiang X., Zu H., Wang W., Feng R. (2021), Nondestructive assessment of microcracks detection in cementitious materials based on nonlinear ultrasonic modulation technique, *Construction and Building Materials*, **267**: 121653, doi: 10.1016/j.conbuildmat.2020.121653.

21. Yang X. *et al.* (2020), Multi-layer polymer-metal structures for acoustic impedance matching in high-frequency broadband ultrasonic transducers design, *Applied Acoustics*, **160**: 107123, doi: 10.1016/j.apacoust.2019.107123.

22. Zhang J., Sun M., Hou D., Li Z. (2017), External sulfate attack to reinforced concrete under drying-wetting cycles and loading condition: Numerical simulation and experimental validation by ultrasonic array method, *Construction and Building Materials*, **139**: 365–373, doi: 10.1016/j.conbuildmat.2017.02.064.